ON-LINE ROBUST MODAL STABILITY PREDICTION USING WAVELET PROCESSING

Martin J. Brenner
Aerospace Engineer

Rick Lind
National Research Council Postdoctoral Research Fellow

NASA Dryden Flight Research Center
Edwards, California

A98-31609

Abstract

Wavelet analysis for filtering and system identification has been used to improve the estimation of aeroservoelastic stability margins. The conservatism of the robust stability margins is reduced with parametric and nonparametric time-frequency analysis of flight data in the model validation process. Nonparametric wavelet processing of data is used to reduce the effects of external disturbances and unmodeled dynamics. Parametric estimates of modal stability are also extracted using the wavelet transform. Computation of robust stability margins for stability boundary prediction depends on uncertainty descriptions derived from the data for model validation. The F-18 High Alpha Research Vehicle aeroservoelastic flight test data demonstrates improved robust stability prediction by extension of the stability boundary beyond the flight regime. Guidelines and computation times are presented to show the efficiency and practical aspects of these procedures for on-line implementation. Feasibility of the method is shown for processing flight data from time-varying nonstationary test points.

Nomenclature

a	wavelet scale
a_i	indexed scale values
A	residue magnitude
ASE	aeroservoelastic
DWT	discrete wavelet transform
e	base of natural logarithms
FFT	fast Fourier transform
$F(P, \Delta)$	feedback interconnection structure
g	wavelet basis function
$G_{a, \tau}$	spectrum of wavelet g
HARV	High Alpha Research Vehicle
i	imaginary unit
$k(t)$	envelope signal of $x(t)$
K	feedback control system
OBES	onboard excitation system
P	nominal plant model
$\hat{P}$	updated plant model
$P(s)$	Laplace transform of system
$\hat{P}(s)$	estimate of $P(s)$
$\bar{q}$	dynamic pressure
s	Laplace frequency
t	time
u	system input
$W(a, \tau)$	WT with scale a and translation time τ
$W(a_i, \tau)$	WT with scale a_i and translation time τ
WT	wavelet transform
W_g	continuous WT with basis g
W_{add}	weighting on Δ_{add}
W_{in}	weighting on Δ_{in}
$x(t)$	time-domain signal
$\hat{x}(t)$	filtered time-domain signal
$X(\omega)$	frequency-domain signal
$\hat{X}(\omega)$	estimate of $X(\omega)$
$X(\tau, \omega)$	wavelet-transformed signal
$\hat{X}(\tau, \omega)$	filtered wavelet-transformed signal
y	system output
γ	frequency step constant
Γ	robust stability margin
$\delta_{\bar{q}}$	uncertainty in flight condition
Δ	uncertainty operator
$\hat{\Delta}$	estimate of Δ

Δ_{add}	uncertainty at output
Δ_{in}	uncertainty at input
Δ_A	modal parametric uncertainty
ζ	damping ratio
μ	structured singular value
τ	wavelet translation time
$\phi(t)$	signal phase
ϕ_o	constant phase lag
ω	radian frequency
ω_d	modal damped frequency
ω_n	natural frequency
ω_o	wavelet peak frequency
$*$	complex conjugate
$\angle$	phase angle
$\mid\ \mid$	modulus
$\|\ \|_\infty$	operator infinity norm

Introduction

Envelope expansion of new or modified aircraft often requires structural stability testing to verify safety margins to prevent against aeroservoelastic (ASE) instability. In-flight testing allows determination of aeroelastic or ASE effects as a function of flight parameters. Flight data are acquired for stability estimation and system identification to compare with analytic predictions. Any anomalies are regarded with care for safety of flight.

Excitation systems are often essential to establish stability trends from noisy measurements because atmospheric turbulence is generally insufficient to provide adequate levels of excitation.[1] These systems often generate deterministic, nonstationary input signals. When applied as filter banks for data enhancement, wavelet signal processing has shown promise for system identification in such environments. Improvement in flight data analysis is achieved by discriminating areas of low signal-to-noise ratio, unmodeled dynamics, and external disturbances. Removing aspects of signal responses detrimental to linear identification methods may improve stability tracking with time-frequency filtering.[2-4]

Wavelet transforms have also been applied to parametric identification of time-varying multiple-degree-of-freedom systems by estimating the impulse response using correlation methods.[5, 6] Modal frequency and damping parameters are estimated directly from the data without intermediate model identification schemes. In these schemes, parameter range approximations are necessary to discriminate frequency and damping.

A recent method[7] uses a wavelet transform (WT) on free-response data to directly supply information on time-dependent modal decay rate and phase variation. Without any approximation of parameter range, natural frequencies and damping ratios are extracted from the response. Damping and frequency trends are useful for noting changes in system dynamics as a function of flight condition, thereby helping to reduce conservatism in real parameter variations of the uncertainty model.

Model validation is a critical procedure in the computation of robust stability margins. The margins are adversely affected by poor characterizations of the uncertainty size and structure, which are determined by perturbation magnitude, location in the system, and type (real or complex). Wavelet processing of ASE flight test data improves the robust stability margin estimate by helping to reduce the conservatism in the uncertainty description pertaining to complex (nonparametic) and real (parametric) perturbations.

This paper discusses augmenting wavelet filtering with wavelet-based modal parameter extraction to produce robust stability margins with reduced-norm uncertainty sets of complex (nonparametric) and real (parametric) perturbations. The decrease in conservatism results in a more practical and valuable robust stability margin than stability margins without reduced-norm uncertainty sets.

Transfer functions and modal parameter estimates derived from time-frequency Morlet wavelets are used to estimate state-space ASE models from the F-18 High Alpha Research Vehicle (HARV)[8] (fig. 1) flight data. These models are used in a robust stability boundary prediction method based on the structured singular value, μ.[9] On-line implementation issues are presented to demonstrate feasibility and efficiency in a real-time test environment.

The F-18 High Alpha Research Vehicle and Aeroservoelastic Flight Test

The F-18 HARV aircraft is a two-seat fighter that was modified to include thrust-vectoring paddles on the engines and a research flight control system to ensure stability at high-angle-of-attack flight conditions.[10] The flight system also included an excitation signal generator, the onboard excitation system (OBES), for aerodynamic parameter identification, closed-loop stability monitoring, and ASE excitation.[11] For ASE

stability monitoring, the OBES was configured to sum programmed digital signals to the control system actuator commands for structural excitation of the primary modes (table 1). Inputs from 5 to 20 Hz were added to the control surface commands at angles of attack from 5° to 70° at 1 g.

EC96-43595-2

Figure 1. F-18 High Alpha Research Vehicle.

Table 1. F-18 HARV calculated elastic frequencies.

Antisymmetric Mode	ω, Hz
Fuselage first bending	7.1
Wing first bending	8.8
Wing first torsion	12.0
Stabilizer first bending	13.6
Wing fore-aft	15.2
Fin first bending	15.7
Fuselage first torsion	19.1
Fuselage second bending	21.4
Exhaust vane rotation	22.1
Inboard flap rotation	23.2
Fore-fuselage torsion	24.2

Analytical predictions indicated poor ASE stability robustness in the lateral-directional feedback loops. Structured singular values of complementary sensitivity near the first antisymmetric wing bending and wing torsion modes (approximately 9 Hz and 12 Hz, respectively) approached 0 dB, and the wing fore-aft

mode at approximately 15 Hz was at −6 dB. Flight envelope limits were at altitudes of 15,000–35,0000 ft and a maximum speed of Mach 0.7. Worst-case flight conditions from the analysis were at speeds less than Mach 0.3, altitudes higher than 30,000 ft, and angles of attack greater than 50°. This paper addresses robust stability at a representative worst-case flight condition of 50° angle of attack at Mach 0.3 and an altitude of 30,000 ft.

Time-Frequency System Identification

A desirable feature of signal analysis is adaptation to both transient and stationary characteristics, which implies both time- and frequency-domain resolution criteria subject to the uncertainty principle. These competing requirements demand a method that is tunable according to the local signal dynamics. For general types of input excitation, constant time-frequency resolution analysis[2, 3, 12] may not be applicable.

Redundant, continuous wavelet transform methods give arbitrarily good resolutions but are cumbersome[13] and often slow[14] for reconstruction and filtering. Alternatively, nonredundant (compact and orthonormal) wavelet transforms are fast and accurate but are limited in frequency resolution even with wavelet packets. Good frequency resolution is obtained with classical harmonic wavelets,[15] but time resolution is sacrificed. The objective of adjusting the competing requirements of time and frequency resolution with fast, accurate processing is accomplished with a combination of compact orthogonal and harmonic wavelet properties in the compact harmonic wavelets.[13, 16]

Nonparametric Estimation: Wavelet Filtering

The multivoice wavelet transform was introduced to exploit multiresolution analysis using compact harmonic wavelets.[13, 17] "Multivoice," or "multiscale," refers to redundant representations of signals on multiple frequency bands.[18] Nonorthonormal Morlet wavelets are approximated with (harmonic-like) discretizations on multiple wavelet scales. These wavelets form a nonorthogonal redundant basis for the signal space that does not admit a multiresolution analysis. The discrete wavelet transform (DWT) needs to be derived from the wavelet basis to get a multiresolution analysis of the sampled continuous Morlet transform.[17]

The DWT is implemented as a filter bank covering a predefined range of frequencies with corresponding number of frequency bands (voices) for each octave. Interpolation, or scaling, filters are introduced to define how the scales relate to each other in a dyadic fashion for the multiscale representation. These scaling filters are

compact (finite impulse response) for fast and accurate reconstruction. Therefore, multivoice transforms provide practical, fast, and flexible means for analysis and filtering of nonstationary data and enable tunable frequency resolution and time localization.

The wavelet transform of signal $x(t)$ over the time-scale (τ, a) plane is represented as

$$W_g(\tau, a) = \frac{1}{\sqrt{a}} \int x(t) g^* \left(\frac{t - \tau}{a} \right) dt,$$

where scale parameter a is proportional to the duration and inversely proportional to the peak frequency ω_o of the complex Morlet wavelet

$$g(t) = \frac{1}{\sqrt{2\pi}} e^{-\frac{t^2}{2}} e^{i\omega_o t}.$$

The spectrum of a dilated and translated Morlet wavelet

$$G_{a, \tau}(\omega) = e^{-(a\omega - \omega_o)^2} e^{i\omega\tau} \qquad (1)$$

reaches a maximum value at $a = \dfrac{\omega_o}{\omega}$. Frequency discretization is logarithmic in the frequency range of interest by setting the sequence of scale values to $a_i = a_0 \gamma_i$, where ($\log \gamma, \gamma > 1$) is the constant frequency step. Integration step $\log \gamma_i$ is chosen to be small enough that the frequency bandwidth of the scaled wavelets $g_i(t) = \dfrac{1}{a_i} g \left(\dfrac{t}{a_i} \right)$ will appreciably overlap.

A time-scale representation of data is often called a scalogram,[19] which is actually the power spectral density $|W_g(\tau, a)|^2$ of the signal over the (τ, a) plane. Figure 2 shows example scalograms of a 5–20 Hz F-18 HARV aileron chirp (linear frequency sweep) input command (fig. 2(a)) and lateral acceleration feedback response at 50° angle of attack (fig. 2(b)) (note the log frequency scale).

Time-frequency masking of input and output is performed along the sweep. Figure 2 shows this filtering procedure on the input (fig. 2(a)) and output (fig. 2(c)) as processed scalograms. Onboard excitation system inputs are relatively clean because the inputs are digitally generated by the flight system, so time-frequency filtering of the output will be more significant in this case. Figure 3 shows the effect of filtering on the responses. Note that effective signal reconstruction from the processed scalograms is accomplished from the real wavelet basis.
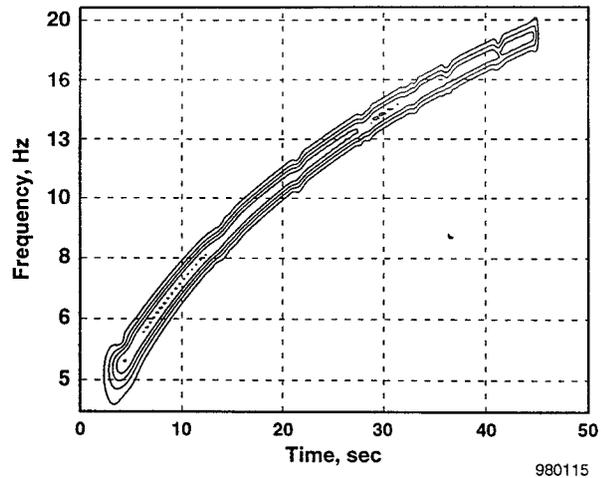
(a) OBES aileron command input.
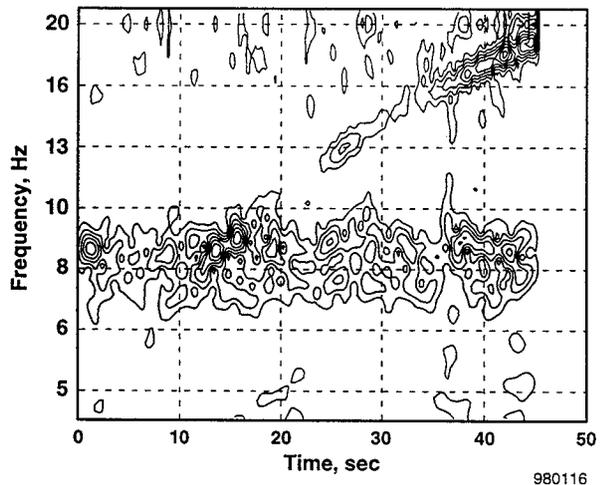
(b) Raw lateral acceleration response.
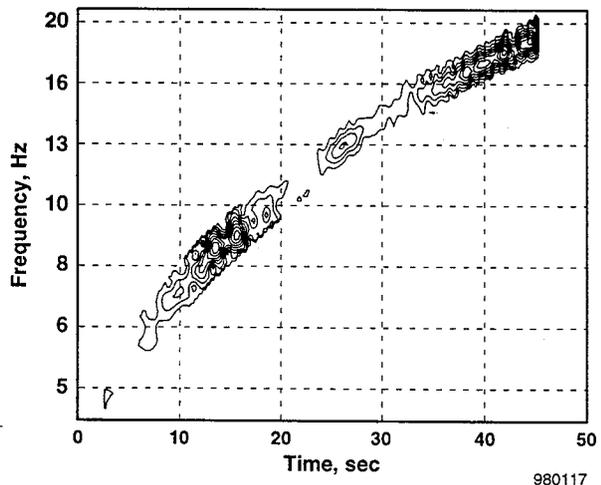
(c) Cleaned lateral acceleration response.
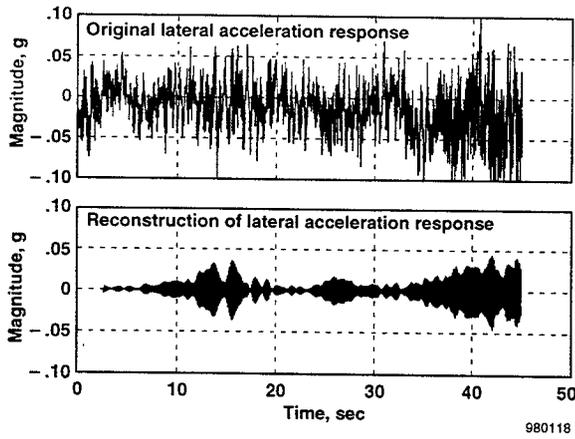
Figure 2. Scalogram contours

4

Figure 3. Responses of original (top) and filtered (bottom) lateral acceleration from OBES aileron command input.

Parametric Modal Estimation: Morlet Wavelet Transform

Modal parameters can be estimated with wavelets by analysis of the system impulse response[7, 20] (appendix). The DWT of a signal using the complex Morlet wavelet is a complex-valued matrix whose modulus and phase are related to impulse response parameters. In the current application, this procedure is applied at every time point assuming at each instant that the response is a sum of multiple-degree-of-freedom impulse responses.

Figure 4 shows an example of response frequency estimation using the linear phase variation of the WT for the filtered lateral acceleration response from aileron input command at 50° angle of attack (using data shown in figure 3). The raw estimate shown at the top of figure 4 corresponds to the derivative of the phase variation of the WT between 20 and 27 sec. Hence, this estimate is of instantaneous frequency from equation 3. Data spikes are removed by limiting values of the second derivative below some threshold. The refined estimate shown at the bottom of figure 4 is computed from the data shown at the top of figure 4 with spikes removed, and these computations are used to derive an approximate response frequency of 11.8 (±0.3) Hz over the respective time span. Wavelet modulus decay is similarly used to derive decay rate.

Figure 5 shows some results of wavelet-based modal estimation using the data from the wavelet-filtered results of figure 3. The upper left of figure 5 shows the mean value of the instantaneous frequency $\phi(t)$, or estimated ω_d, as a function of the complex Morlet wavelet frequency ω_o. The upper right of figure 5 shows plots of

the estimated decay rate, or frequency $\zeta\omega_n$, also as a function of ω_o. From these two parameters are derived the modal natural frequency ω_n and modal damping ratio ζ as functions of ω_o (shown in the lower left and right plots).
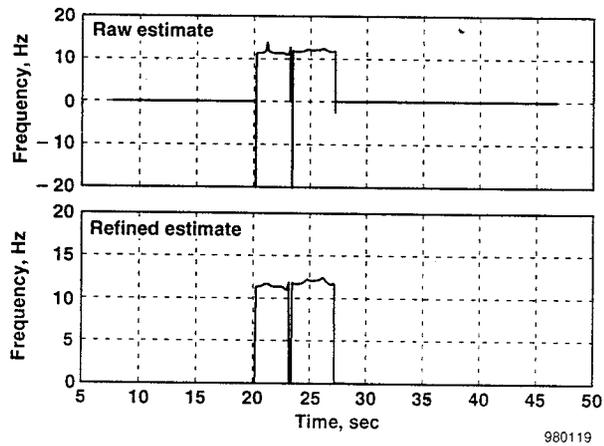

Figure 4. Instantaneous frequency estimation: raw estimate (top) and refined estimate (bottom).
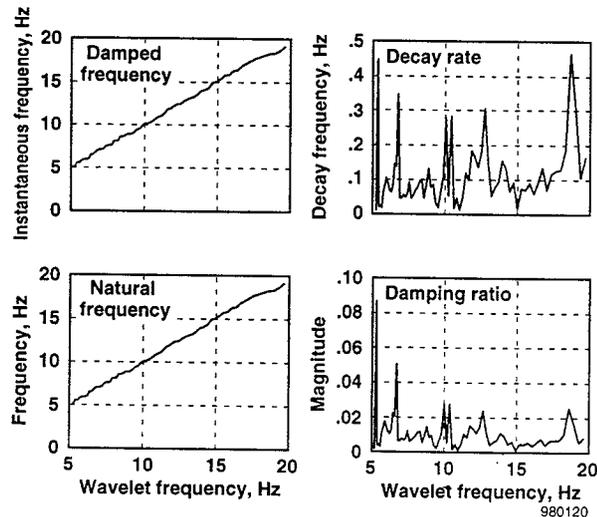

Figure 5. Modal frequency and damping estimates: damped frequency as a function of wavelet frequency (upper left), decay rate as a function of wavelet frequency (upper right), natural frequency as a function of wavelet frequency (lower left), and damping ratio as a function of wavelet frequency (lower right).

Finally, the bank of Morlet wavelets used for natural frequency and damping ratio estimation are tagged for starting time and duration to get the modal estimates as functions of time. Figure 6 shows time-dependent modal parameter estimates. In this case, modal frequency is observed to be essentially the tracked input frequency

because the cleaned output signal shown at the bottom of figure 3 is being used, and this response tends to track the input frequency. From the scalogram shown at the bottom of figure 2, the response lacks definition between 20 and 25 sec and between 32 and 34 sec. These gaps also correspond to the lower output signal levels at these time intervals shown at the bottom of figure 3. Lack of observability makes the modal damping results shown at the right in figure 6 questionable in these particular intervals.
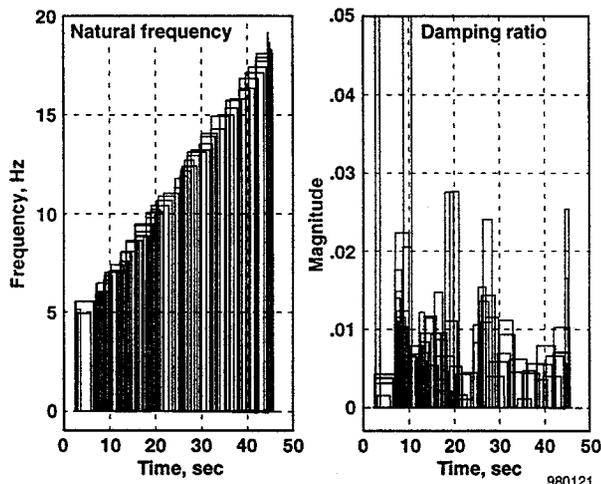

Figure 6. Response natural frequency (left) and damping ratio (right) estimates.

Scalogram contours shown in figure 2 suggest the wavelet coefficients as a measure of data quality and modal definition. In figure 7, the wavelet coefficients are represented for each modal frequency and damping ratio using the same data from the wavelet-filtered results shown in figure 3. Lower magnitude coefficients indicate less observable modal dynamics from the data. Views along each axis in figure 8 show that the coefficients from modal frequency estimates may be used to distinguish more dominant from less observable dynamics. This criterion can be exploited to extract the corresponding modal damping values.[20]

An important point is that the Morlet wavelets are being used to estimate the modal parameters; therefore, an implicit filtering process is being performed independent of the explicit procedure previously described. The wavelet basis representation of the signal is itself a noise-free subspace of the signal function space, and the modal parameters are derived from this signal subspace.
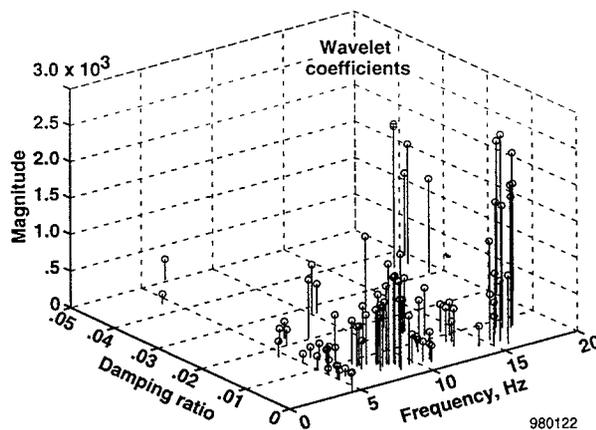

Figure 7. Wavelet coefficient magnitudes as functions of estimated modal frequency and damping estimates.
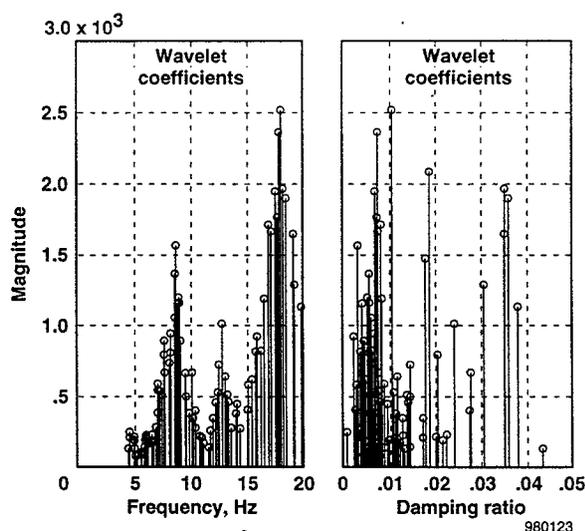

Figure 8. Two-dimensional axial views of wavelet coefficient magnitudes as functions of estimated modal frequency (left) and modal damping ratio (right).

The Structured Singular Value Method

A method to compute stability margins of ASE systems has been formulated based on robust stability theory.[21] This method uses a set of structured operators Δ, referred to as uncertainty, to describe errors and unmodeled dynamics in an analytical model. The structured singular value, μ, is used to compute a stability margin for this model that is robust, or worst-case, to the uncertainty operators.[22]

The μ framework represents systems as operators with interconnections known as linear fractional

6

transformations. This paper uses the notation $F(P, \Delta)$ to represent a feedback interconnection of the plant P and uncertainty operator Δ. Aeroservoelastic systems may have errors affecting different dynamic subsystems, so the Δ is structured such that the feedback interconnections ensure each subsystem is affected by the proper component of Δ.

Flight data can be incorporated into the μ method by formulating an uncertainty description that accounts for observed variations and errors.[23] A model validation analysis is performed on the plant model to ensure the range of dynamics admitted by the uncertainty is sufficient to cover the range of dynamics observed with the flight data. Thus, a robust stability margin is computed that directly accounts for flight data.

An ASE stability margin, Γ, is determined by computing μ with respect to an uncertainty description, $\delta_{\bar{q}}$, that admits variations in dynamic pressure, $\bar{q}$, and an uncertainty description, Δ, that describes modeling errors.[24] This margin relates the largest change in dynamic pressure that may be considered while guaranteeing the plant model is robustly stable to all errors described by Δ.

The Structured Singular Value Method with Wavelet Processing

The μ method can be coupled with the wavelet filtering processes of parametric and nonparametric estimation discussed previously. This coupling is achieved by introducing several time-frequency operations based on wavelet filtering into the basic process. Figure 9 shows the general information flowchart for the μ method with wavelet filtering.
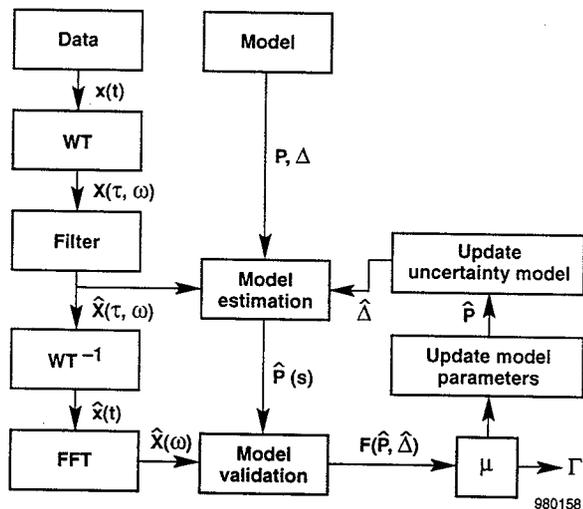

Figure 9. Flowchart of μ method combined with wavelet filtering for on-line wavelet-μ method of robust stability margin analysis of ASE dynamics.

Wavelet transform operations are introduced to process the time-domain data, $x(t)$, before a frequency-domain representation, $\hat{X}(\omega)$, is computed. These operations map the time-domain data into a time-frequency–domain scalogram through a wavelet transform and then map a scalogram back into the time domain through an inverse wavelet transform. A time-frequency filtering process operates between the WT and inverse WT to remove unwanted features from the scalogram before the inverse WT computes a time-domain signal, $\hat{x}(t)$.

A modal parameter estimation operation is introduced using the wavelet algorithm. Properties of the system dynamics are derived from the filtered scalogram. The elements of a nominal plant model, P, are updated with these parameter estimates, and a new plant model, $\hat{P}$, is used to represent the ASE dynamics.

The final operations of the μ method are traditional robust stability operations that operate on frequency-domain data. The effect of the wavelet filtering is to use the filtered versions of the data and plant model for the modal validation. Thus, a new uncertainty operator, $\hat{\Delta}$, is associated with the parameter updated plant, $\hat{P}$, to account for errors observed from the filtered data, $\hat{x}(t)$. A robust stability margin, Γ, is computed that describes the largest change in dynamic pressure for which $\hat{P}$ is robustly stable to the errors $\hat{\Delta}$.

The Structured Singular Value Method with Parameter Estimation

Figure 9 shows an implementation of the μ method with modal parameter estimation. The filter operation for this implementation is ignored, so the wavelet map $\hat{X}(\tau, \omega)$ is equivalent to the original map $X(\tau, \omega)$.

The wavelet-based method for parametric estimation is used to analyze the wavelet map $\hat{X}(\tau, \omega)$ of the flight data. This method estimates modal parameters to describe the system dynamics that generated the flight data. A plant model, $\hat{P}_1$, is computed by updating elements of the nominal plant model, P_0, with the modal parameter estimates. Only a limited subset of dynamics will be observable in the data, so only a correspondingly limited subset of the plant modal parameters will be updated.

An uncertainty description, $\hat{\Delta}_1$, is generated for the plant with updated modal parameters, $\hat{P}_1$, using the model validation procedure. This procedure essentially uses the original flight data measurements because the WT and inverse WT operations will cancel each other except for numerical inaccuracies. Thus, $x(t)$ approximately equals $\hat{x}(t)$, and an uncertainty description is computed for the updated plant that

accounts for all variations and anomalies in the recorded data.

The magnitude of uncertainty associated with the updated plant should be less than (or equal to) the uncertainty magnitude associated with the nominal plant. This decrease in uncertainty results from the ability of the updated plant to account for bias in the nominal plant estimates. Hence, the uncertainty associated with the updated parameter is less than the uncertainty associated with the nominal parameter. Thus, $\|\hat{\Delta}_1\|_\infty \le \|\Delta_0\|_\infty$.

The conservatism in robust stability margins computed by the μ method arises from the excessive uncertainty needed to account for errors in a model. A decrease in uncertainty from model updating with the parameter estimation process should decrease this conservatism.

The Structured Singular Value Method with Wavelet Filtering and Parameter Estimation

Another implementation of the μ method with modal parameter estimation results from including a nontrivial filtering operation (fig. 9). The wavelet filtering operation, which is a type of nonparametric estimation, is used to generate scalograms to represent desired features of input and output data in the time-frequency domain. The filtered scalogram, $\hat{X}(\tau, \omega)$, may be arbitrarily different than the original scalogram, $X(\tau, \omega)$, depending on the energy of the signal components that do not correlate to desired features.

The filtered wavelet map is input to the parametric estimation process. Resulting modal parameter estimates represent the dynamics of the system model that generate the desired features dominant in the filtered maps. The elements of the nominal plant model, P_0, are replaced with the modal parameter estimates to generate an updated plant model, $\hat{P}_2$.

The filtered wavelet map is also used to generate an uncertainty description for the updated plant $\hat{P}_2$. A time-domain signal, $\hat{x}(t)$, which represents the filtered measurement data, is computed by an inverse wavelet transform on the filtered scalogram. A frequency-domain representation of this filtered signal is computed from a Fourier transform and is used by the model validation process. The resulting uncertainty, $\hat{\Delta}_2$, describes the variations between the updated plant $\hat{P}_2$ and the filtered data.

The uncertainty description size (in norm) associated with $\hat{P}_2$ should be reduced from that used to validate the unfiltered data when used for validating the filtered data. The filtering process should remove nonlinearities and harmonics along with noise that causes aliasing and errors in measured transfer functions. This removal of errors may decrease the variance in modal parameter estimates so that an updated model can be generated with less uncertainty. The filtered data generate parameters that are less scattered than the parameters generated from the unfiltered data, thereby allowing the uncertainty ball to be smaller than for the unfiltered case, so $\|\hat{\Delta}_2\|_\infty \le \|\hat{\Delta}_1\|_\infty \le \|\Delta_0\|_\infty$. Therefore, the conservatism in robust stability margins computed by the μ method may be decreased by including the wavelet filtering into the process.

Aircraft Models and Uncertainties

Robust stability margins for the ASE dynamics of the F-18 HARV are computed using the μ method with wavelet filtering. Stability margins are computed for the antisymmetric modes (table 1) of the lateral-directional ASE dynamics for the aircraft at Mach 0.3 and an altitude of 30,000 ft ($\bar{q} = 41$ lb/ft^2) at 50° angle of attack. A baseline implementation of the μ method indicates these margins may lie within the flight envelope, so any reduction in conservatism could be significant at this flight condition.[15]

An uncertainty description is formulated using three operators to describe errors in an F-18 HARV analytical model. A complex operator, Δ_{in}, is a multiplicative uncertainty in the control inputs to the plant and accounts for actuator errors and unmodeled dynamics. Another complex operator, Δ_{add}, relates the control inputs to the feedback measurements to account for uncertainty in the magnitude and phase of the computed plant responses. The remaining uncertainty operator, Δ_A, is a real parametric uncertainty affecting the modal parameters of the open-loop state matrix to describe errors in natural frequency and damping parameters.

Figure 10 shows the block diagram for robust stability analysis of the F-18 HARV ASE dynamics. This figure includes an operator, $\delta_{\bar{q}}$, that affects the nominal dynamics to describe changes in flight condition and is used to interpret μ as a stability margin.[11] Additional operators, W_{add} and W_{in}, are shown as weightings to normalize the frequency-varying uncertainty operators, Δ_{add} and Δ_{in}. The system model also contains 2-percent sensor noise corruption on each measurement.

The lateral-directional controller, K, has 29 states. Table 2 shows the feedback measurements and control inputs associated with this controller.
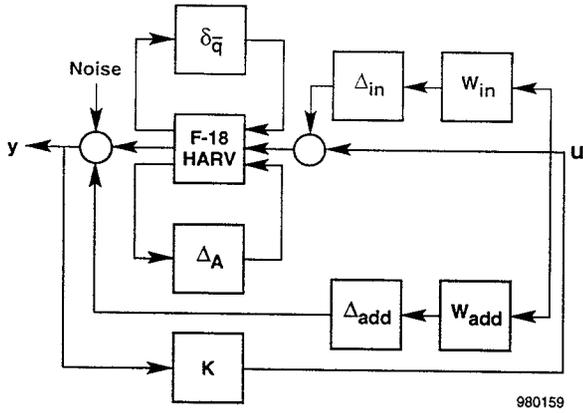
Figure 10. F-18 HARV uncertainty block diagram for robust stability margin analysis.

Baseline Model Validation

A model with an associated uncertainty description was generated to compute robust stability margins by the μ method. The plant model, P_0, is the nominal model generated by a finite-element analysis of the ASE dynamics. The parameters in this model are theoretical and have not been updated by analysis of flight data. The model contains seven antisymmetric elastic structural modes between 5 and 20 Hz (table 1).

Table 2. Feedback measurements and control commands for the thrust vectoring lateral-directional controller K.

Feedback Measurements	Control Commands
Roll rate	Aileron
Yaw rate	Differential leading edge flap
Sideslip rate	Differential trailing edge flap
Lateral acceleration	Differential stabilator
	Rudder
	Yaw thrust vectoring

An uncertainty description, Δ_0, is generated using the model validation procedure on a frequency-domain representation of the unfiltered data. Only the observed energies from frequencies less than 20 Hz are used for validation because considerable energy exists at frequencies of approximately 20 Hz caused by structural dynamics associated with the thrust-vectoring vane system that is difficult to model. The primary transfer function used in the derivation of the uncertainty description is the lateral acceleration response from yaw thrust vectoring. These data responses demonstrate good observability of the primary modes to a maximum 20 Hz.

Separate parametric uncertainty levels are chosen for each mode of the open-loop state matrix to reflect different levels of accuracy. These uncertainty magnitudes are computed to describe observed variations between the model transfer function and the flight data measurements. Table 3 shows the nominal modal parameters and the amount of variation admitted by the parametric uncertainty.

Table 3. Modal parameters and uncertainty variations for model P_0 and Δ_0.

Mode	ω, Hz	ζ
Fuselage first bending	6.85 ± 0.07	0.012 ± 0.006
Wing first bending	8.96 ± 0.18	0.006 ± 0.004
Wing first torsion	12.84 ± 0.13	0.011 ± 0.006
Wing fore-aft	15.69 ± 0.63	0.010 ± 0.007
Fuselage first torsion	18.86 ± 0.76	0.010 ± 0.005

The amount of variation needed to describe modal parameter errors is fairly significant for all modes, especially in damping ratio. The fuselage first torsion and wing fore-aft modes have properties that are particularly poorly modeled, so as much as 4-percent error exists in natural frequency and 70-percent error in damping. The remaining modes have only 2-percent error in natural frequency but still require at least 50-percent error in damping.

The weighting functions for the input multiplicative and additive uncertainties are chosen to account for any errors between the model and the flight data that cannot be covered by the parametric modal uncertainty.

$$W_{in} = 10\frac{s + 100}{s + 5000}$$

$$W_{add} = 0.02$$

Model Validation with Parameter Estimation

The parametric modal estimation procedure was used to process the flight data and compute modal parameters for an analytical model. This procedure uses equation 2 to generate estimates of the modal parameters from the unfiltered wavelet map $X(\tau, \omega)$ and associated properties.

A plant model, P_1, is computed that is the estimated plant model obtained from the wavelet filtering. This model is formulated initially as the nominal plant P_0, but certain theoretical modal parameters are replaced by their estimated values. Table 4 shows the nominal values of these parameters. The natural frequencies are not changed by more than 1 Hz for any of the estimated modes; however, the estimated damping parameters are significantly higher than the theoretical values.

Table 4. Modal parameters and uncertainty variations for model P_1 and Δ_1.

Mode	ω, Hz	ζ
Fuselage first bending	6.85 ± 0.07	0.012 ± 0.006
Wing first bending	8.60 ± 0.10	0.040 ± 0.021
Wing first torsion	13.31 ± 0.15	0.045 ± 0.024
Wing fore-aft	16.51 ± 0.35	0.045 ± 0.023
Fuselage first torsion	18.21 ± 0.37	0.030 ± 0.010

An uncertainty description, Δ_1, is associated with P_1 to describe the levels of modeling error in this estimated plant. The magnitudes of the parametric modal uncertainty in Δ_1 are chosen by comparing flight data with theoretical transfer functions for P_1. Table 4 shows the ranges of modal parameter variations admitted by this uncertainty.

The variations in natural frequency and dampings are seen to be considerably reduced for $F(P_1, \Delta_1)$ (table 4) compared to the large variations for $F(P_0, \Delta_0)$ (table 3). The estimated modal parameters used in P_1 are much closer to those of the aircraft, so the predicted response of P_1 closely matches the flight data measurements. Thus, the natural frequency errors are all less than 2 percent, and the damping errors are all less than 55 percent.

The weightings, W_{add} and W_{in}, affecting the remaining uncertainties in Δ_1 are identical to those of Δ_0.

Model Validation with Wavelet Filtering and Parameter Estimation

Modal parameters for model estimate $\hat{P}_2$ are extracted from the time-frequency–domain representation of the wavelet-filtered flight data $\hat{X}(\tau, \omega)$. Figure 9 shows this procedure. As shown in table 5, the modal estimates from the filtered data are similar to the unfiltered estimates shown in table 4. Parameter variations resulting from validated model $F(\hat{P}_2, \hat{\Delta}_2)$, however, are reduced in

modal frequency to 1 percent and in modal damping to 10 percent.

Table 5. Modal parameters and uncertainty variations for model P_2 and Δ_2.

Mode	ω, Hz	ζ
Fuselage first bending	6.85 ± 0.07	0.012 ± 0.001
Wing first bending	8.70 ± 0.09	0.035 ± 0.003
Wing first torsion	13.31 ± 0.14	0.045 ± 0.004
Wing fore-aft	16.61 ± 0.17	0.045 ± 0.004
Fuselage first torsion	18.21 ± 0.18	0.040 ± 0.004

Aeroservoelastic Stability Margins

Nominal stability margins are computed for the plant model using the original theoretical modal parameters and for the updated models using parameters estimated from wavelet filtering. These margins are computed from a μ analysis with respect to the variation in dynamic pressure, $\bar{q}$, but ignoring the modal and complex uncertainty operators. The nominal stability margins, Γ (table 6), demonstrate the largest decrease relative to the nominal dynamic pressure of $\bar{q} = 41$ lb/ft^2 that may be considered before the models incur an ASE instability. Therefore, a larger negative value of stability margin indicates a greater margin of robust stability than a value closer to zero does.

Table 6. Nominal stability margins for models.

Model	Γ	ω
$F(P_0, 0)$	-268 lb/ft^2	14.8 Hz
$F(P_1, 0)$	-368 lb/ft^2	14.8 Hz
$F(P_2, 0)$	-379 lb/ft^2	14.8 Hz

The original theoretical model has a nominal stability margin of $\Gamma = -268$ lb/ft^2 resulting from a critical instability of the wing fore-aft mode at 14.8 Hz. The margins are increased by updating the models with modal parameters estimates; however, the wing fore-aft mode remains the critical mode for these updated models. This increase in stability margin associated with wavelet filtering is not guaranteed to occur for all applications; rather, the filtering is designed to increase nominal model accuracy. The nominal model for the F-18 HARV has excessively low damping values

compared to the damping levels resulting from the wavelet filtering. Increasing damping ratio estimates make the plant effectively more stable and increase the stability margins.

These nominal margins are all greater in absolute value than the nominal dynamic pressure, thus demonstrating the nearest instability to the flight envelope occurs at a negative dynamic pressure, which is physically unrealizable. Therefore, the nominal dynamics are free of ASE instabilities within the research flight envelope.

Robust stability margins are computed with respect to the uncertainty description (fig. 10) (table 7). Model $F(P_0, \Delta_0)$ describes the original model with parameter variations (table 3). The model with modal parameter estimates, $F(P_1, \Delta_1)$, has the reduced uncertainty levels leading to the variations shown in table 4. The remaining model, $F(P_2, \Delta_2)$, describes the model formulated by combining wavelet filtering with parameter estimation and introducing uncertainty to allow the variations shown in table 5.

Table 7. Robust stability margins for models with respect to uncertainty descriptions.

Model	Γ	ω
$F(P_0, \Delta_0)$	-4 lb/ft^2	5.4 Hz
$F(P_1, \Delta_1)$	-222 lb/ft^2	7.0 Hz
$F(P_2, \Delta_2)$	-239 lb/ft^2	7.0 Hz

The stability margin of the original model is strongly affected by considering uncertainty. This margin is reduced from $\Gamma = -268$ lb/ft^2 for the nominal dynamics to $\Gamma = -4$ lb/ft^2 for the dynamics with respect to uncertainty. The critical mode remains the wing fore-aft mode despite the uncertainty; however, the dynamic pressure at which this mode becomes unstable is quite different. This robust stability margin demonstrates the nominal model may be misleading and the nearest unstable flight condition may actually lie within the flight envelope.

The robust stability margin for the model $F(P_1, \Delta_1)$, using modal parameter estimates, is significantly larger than the margin of the original system. The wavelet processing is able to identify a more accurate model with less associated uncertainty, so the conservatism in the margin is reduced. The robust stability margin for this model is $\Gamma = -222$ lb/ft^2 and indicates the nearest instability for the updated model. Despite the range of dynamics incurred by uncertainty, the margin is at a

negative dynamic pressure, and so the flight envelope is free of ASE instabilities.

The critical mode associated with the robust stability margin for the updated model is the fuselage first bending mode. This mode differs from the critical wing fore-aft mode associated with the nominal margin. This shift in critical mode is a result of modal parameter updates and corresponding reduced uncertainty sets.

The model formulated from parameter estimation coupled with wavelet filtering, $F(P_2, \Delta_2)$, has a robust stability margin similar to the margin of $F(P_1, \Delta_1)$. The magnitude of this margin is slightly higher as a result of the reduced uncertainty levels needed to validate the filtered flight data; however, the critical mode remains the fuselage first bending mode.

Reduction in parameter variations from nonparametric wavelet filtering did not have as much an effect on robust stability as the updated parameter estimates. Nonparametric filtering has more impact on parameter variance, which was a less significant factor than parameter bias.

To summarize, comparison between the nominal results (table 6) and the robust margins (table 7) shows that the decrease in margin from uncertainty is clearly evident. The decrease is most substantial for plant model P_0, which has the greatest amount of modal uncertainty in Δ_0, yet the frequency of instability is consistent with the nominal cases. When updated modal parameter estimates are incorporated in P_1 and P_2, the decrease in margins are less than the nominal models because of the smaller uncertainty sets (Δ_1, Δ_2) compared to Δ_0.

The main difference between nominal and robust results is in modal frequency of instability. Wing fore-aft modal frequency increased approximately 1 Hz from its theoretical value to the updated value, and thereby became a less significant factor in the stability margin calculation compared with fuselage first bending. This result confirms that the effect of parameter estimation, and essentially data quality, in model validation becomes a critical factor in robust stability boundary prediction.

On-Line Implementation

Analysis of flight data in an on-line environment requires interactive capabilities. In reference to the flowchart shown in figure 9, the data stream is first wavelet-processed to provide information to the model validation step. Wavelet processing will require resolution criteria, filtering options, and a methodology for extracting dominant dynamics (fig. 7). A robust

stability margin is then calculated based on the model validation test. Modal parameters can be incorporated into a model update, and uncertainty descriptions are modified accordingly. Finally, an updated model $\hat{P}(s)$ is created to close the loop until the next data stream is processed. A parallel effort of wavelet processing of future data while model updating from past data is therefore possible.

Model updates need to be performed in the context of the test scenario, flight conditions, and stability criteria.[9] Modal parameters from recent (local) tests can be used if stability prediction is based on a particular sequence of adjacent test conditions. This approach attempts to minimize conservatism for a particular area of the flight envelope or a particular flight regime. Alternatively, model uncertainty may be continuously increased in a worst-case approach to assure that all nominal models with the associated uncertainty description are not invalidated by any of the data sets. In this case, a single global uncertainty model is generated for conservative measures. A hybrid approach would segment areas of the flight envelope for a combination of local analyses in which each would have some flight condition commonality.

Computation requirements are reasonable. A 200-MHz computer is able to wavelet-process 1 min of 100-Hz data for one input-output pair of channels and five (octave) wavelet resolution levels in 3–5 min of central processing unit time. This amount is comparable to the time needed to compute the model validation and μ step in a worst-case analysis for flutter prediction,[25] and the μ step does not depend on the data access parameters. Hence, a parallel computation is feasible within 3–5 min. However, with a recently developed real-time wavelet processor,[26] the entire on-line wavelet-μ process can be computed serially within a worst-case 3-min time window.

Conclusion

Improvements in aeroservoelastic flight data analysis and stability prediction estimation have been presented. Wavelet approaches to system identification have been applied by combining filtering and parametric time-frequency identification algorithms with Morlet wavelets. The combination of these estimation schemes extracted modal estimates and system uncertainty representations for less conservative model validation. Uncertainty ranges validated by F-18 High Alpha Research Vehicle aeroservoelastic data were shown to decrease by incorporating modal estimates based on the wavelet-processed data.

With the model parameter and uncertainty description updates, the critical aeroservoelastic instability changed in modal frequency and flight condition. A predicted instability within the flight envelope using an uncertain baseline model was found to be too conservative. Model updates pushed the instability beyond the flight regime. The ultimate objective of predicting stability boundaries from flight data was enhanced by a reduction in conservatism of the stability margin estimates. On-line implementation issues and computation time were presented to demonstrate feasibility in an actual flight test situation.

APPENDIX

Given a general harmonic signal,

$$x(t) = k(t)\cos(\phi(t)t),$$

the wavelet transform (WT) of $x(t)$ is

$$W(a, \tau) = \sqrt{a}k(t)e^{-(a\phi(t) - \omega_o)^2}e^{i\phi(t)\tau}.$$

For fixed dilation parameter a_i (equivalently fixed frequency ω), the modulus and phase of the WT of $x(t)$ are

$$\left|W(a_i, \tau)\right| = \sqrt{a_i}k(t)e^{-(a_i\phi(t) - \omega_o)^2}$$

$$\angle\left[W(a_i, \tau)\right] = \phi(t)\tau. \tag{2}$$

Instantaneous frequency of a signal in this case can be expressed as[23]

$$\phi(t) = \frac{1}{2\pi}\frac{d}{dt}(\angle[W(a_i, \tau)]). \tag{3}$$

This expression shows that a general time-varying envelope $k(t)$ or phase $\phi(t)$ of the -signal can be determined from the modulus and phase of the WT for each fixed wavelet frequency.

Specifically, from the impulse response of a single-degree-of-freedom viscous damper

$$x(t) = Ae^{-\zeta\omega_n t}\cos(\omega_d t + \phi_o),$$

substitution of the WT expressions from equation 2 gives

$$k(t) = \frac{\left|W(a_i, \tau)\right|}{\sqrt{a_i}e^{-(a_i\phi(t) - \omega_o)^2}} = Ae^{-\zeta\omega_n t}$$

$$\phi(t)t = \angle\left[W(a_i, \tau)\right] = \omega_d t + \phi_o.$$

For a constant wavelet frequency line corresponding to a_i over time τ in the (a, τ) plane, estimation of the WT linear phase variation (or mean value of the instantaneous frequency over time, shown in equation 3) gives $\phi(t) \approx \omega_d$, and the envelope decay rate is $\zeta\omega_n$. Natural frequency ω_n and modal damping ratio ζ are therefore derived. The WT becomes a complex representation of the original real signal from which the signal eigenvalues are computed without any approximation of their range.

Multiple-degree-of-freedom systems are analyzed similarly by noting that the dilated Morlet wavelet is a band-pass filter (eq. 1). With sufficient resolution of dilation a_i, damped modal frequencies $\omega_{d_i} = \dfrac{\omega_o}{a_i}$ can be discriminated. To recapitulate, the decay rate of the envelope of each mode is calculated from the log-slope of the wavelet modulus decay, and damped modal frequency is estimated as the linear phase variation of the WT as a function of time. Adequate frequency resolution can be enforced with the multiscaled compact harmonic Morlet wavelets

References

[1]Brenner, Martin J., Richard C. Lind, and David F. Voracek, "Overview of Recent Flight Flutter Testing Research at NASA Dryden," AIAA 97-1023 and NASA TM-4792, Apr. 1997.

[2]Brenner, Martin J. and Eric Feron, "Wavelet Analysis of F/A-18 Aeroelastic and Aeroservoelastic Flight Test Data," AIAA 97-1216 and NASA TM-4793, Apr. 1997.

[3]Feron, Eric, Marty Brenner, Jim Paduano, and Arkadiy Turevskiy, "Time-Frequency Analysis for Transfer Function Estimation and Application to the F18-SRA," to be published in *AIAA Journal of Guidance, Control, and Dynamics*, vol. 21, no. 3, May–June 1998.

[4]Xia, Xiang-Gen, "System Identification Using Chirp Signals and Time-Variant Filters in the Joint Time-Frequency Domain," *IEEE Transactions on Signal Processing*, vol. 45, no. 8, Aug. 1997, pp. 2072–2084.

[5]Freudinger, Lawrence C., Rick Lind, and Martin J. Brenner, "Correlation Filtering of Modal Dynamics Using the Laplace Wavelet," *Proceedings of the 16th International Modal Analysis Conference*, vol. 2, Feb. 1998, pp. 868–877.

[6]Lind, Rick, Marty Brenner, and Sydney Haley, "Estimation of Modal Parameters Using a Wavelet-Based Approach," AIAA 97-3836, Aug. 1997.

[7]Ruzzene, M., A. Fasana, L. Garibaldi, and B. Piombo, "Natural Frequencies and Dampings Identification using Wavelet Transform: Application to Real Data," *Mechanical Systems and Signal Processing*, vol. 11, no. 2, Mar. 1997, pp. 207–218.

[8]Bowers, Albion H., Joseph W. Pahle, R. Joseph Wilson, Bradley C. Flick, and Richard L. Rood, *An Overview of the NASA F-18 High Alpha Research Vehicle*, NASA-TM-4772, 1996.

[9]Lind, Rick and Martin J. Brenner, *Robust Flutter Margin Analysis That Incorporates Flight Data*, NASA-TP-1998-206543, Mar. 1998.

[10]Pahle, Joseph W., Bruce Powers, Victoria Regenie, Vince Chacon, Steve Degroote, and Steven Murnyack, *Research Flight-Control System Development for the F-18 High Alpha Research Vehicle*, NASA-TM-104232, 1991.

[11]Brenner, Martin J., *Aeroservoelastic Modeling and Validation of a Thrust-Vectoring F/A-18 Aircraft*, NASA-TP-3647, 1996.

[12]Dalianis, S. A., J. K. Hammond, P. R. White, and G. E. Cambourakis, "Simulation and Identification of Nonstationary Systems Using Linear Time-Frequency Methods," *Journal of Vibration and Control*, vol. 4, no. 1, Jan. 1998, pp. 75–91.

[13]Le, Dzu K., "Applications of Sampling Theorems in Wavelet Spaces to Multiresolution Visualization and Data Segmentation," in *Wavelet Applications in Signal and Image Processing III*, vol. 2569, part 1, Andrew F. Laine and Michael A. Unser, eds., Jul. 1995, pp. 220–233.

[14]Mallat, Stephane and Zhifeng Zhang, "Matching Pursuits With Time-Frequency Dictionaries," *IEEE Transactions on Signal Processing*, vol. 12, no. 41, Dec. 1993, pp. 3397–3415.

[15]Newland, D. E., *An Introduction to Random Vibrations, Spectral and Wavelet Analysis*, 3rd edition, Longman Scientific and Technical, New York, 1993.

[16]Le, Dzu K., Albert K. Owen, and Duane L. Mattern, "Multiscale Analysis of Stall Inception and Instabilities in an Axi-Centrifugal Turboshaft Engine," AIAA-96-3174, Jul. 1996.

[17]Shensa, Mark J., "Discrete Inverses for Nonorthogonal Wavelet Transforms," *IEEE Transactions on Signal Processing*, vol. 44, no. 4, Apr. 1996, pp. 798–807.

[18]Shensa, Mark J., "The Discrete Wavelet Transform: Wedding the À Trous and Mallat Algorithms," *IEEE Transactions on Signal Processing*, vol. 40, no. 10, Oct. 1992, pp. 2464–2482.

[19]Meyer, Yves, *Wavelets: Algorithms and Applications*, translated by Robert D. Ryan, Society for Industrial and Applied Mathematics, Philadelphia, 1993.

[20]Atalla, Mauro J., "On Using the Wavelet Transform to Update Models," *Proceedings of the 16th International Modal Analysis Conference*, vol. 2, Feb. 1998, pp. 1675–1681.

[21]Lind, Rick and Marty Brenner, "Analysis of Aeroservoelastic Stability Margins Using the μ Method," AIAA-98-1895, Apr. 1998.

[22]Packard, Andrew K. and John C. Doyle, "The Complex Structured Singular Value," *Automatica*, vol. 29, no. 1, 1993, pp. 71–109. (Also available at *http://www.math.utwente.nl/eic/*. Accessed March 30, 1998.)

[23]Lind, Rick and Marty Brenner, "Incorporating Flight Data into a Robust Aeroelastic Model," to be published in *AIAA Journal of Aircraft*, vol. 35, no. 3, May–June 1998.

[24]Lind, Rick and Marty Brenner, "Robust Flutter Margins of an F/A-18 Aircraft from Aeroelastic Flight Data," *AIAA Journal of Guidance, Control, and Dynamics*, vol. 20, no. 3, May–June 1997, pp. 597–604.

[25]Lind, Rick C. and Martin J. Brenner, "A Worst-Case Approach for On-Line Flutter Prediction," *International Forum on Aeroelasticity and Structural Dynamics*, vol. 2, June 1997, pp. 79–86.

[26]Miller, Matthew J., Lawrence C. Freudinger, and Martin J. Brenner, "Real-Time Interactive Wavelet Analysis," *Proceedings of the 16th International Modal Analysis Conference*, Feb. 1998, pp. 1581–1586.